International Communications in Heat and Mass Transfer 37 (2010) 1096–1105

Contents lists available at ScienceDirect

International Communications in Heat and Mass Transfer

journal homepage: www.elsevier.com/locate/ichmt

Microwave-assisted heating of cementitious materials: Relative dielectric properties, mechanical property, and experimental and numerical heat transfer characteristics ☆

Natt Makul [a,b,*], Pornthip Keangin [a], Phadungsak Rattanadecho [a,*], Burachat Chatveera [b], Dinesh K. Agrawal [c]

[a] Research Center for Microwave Utilization in Engineering (R.C.M.E.), Department of Mechanical Engineering, Faculty of Engineering, Thammasat University, (Rangsit Campus), Khlong Luang, Prathum thani, 12121, Thailand
[b] Department of Civil Engineering, Faculty of Engineering, Thammasat University, Khlong Luang, Prathum Thani, 12120, Thailand
[c] The Materials Research Institute, The Pennsylvania State University, University Park, PA 16802, USA

ARTICLE INFO

Available online 7 July 2010

Keywords:
Cementitious materials
Hydration
Microwave energy
Strength

ABSTRACT

The characteristics of cementitious materials subjected to microwave energy are presented. First, the dielectric properties of cementitious materials during a 24-hour first-hydration period were measured at a frequency of 2.45 GHz. Second, the characteristics of hardened cement paste as subjected to heating for a short period (without loss of moisture) by microwave energy with a single-mode rectangular wave guide, with specific attention to temperature rise, compressive strength, and the use of the maturity function was investigated experimentally and theoretically. The obtained results show that dielectric properties are relatively high and remain constant during the dormant period. After this period, the hydration reaction resumes and dielectric properties decrease rapidly. With the use of microwave heating, early-age strength increases during the first 14 days; however, during the next 14 days, early-age strength decreases slightly, until it reaches its lowest at the 28-day mark. The temperature rise as actually recorded at the center of the sample during microwave heating in our experiment consistently agreed with figures calculated by a mathematical model.

1. Introduction

By now, microwave (MW) energy has been established as a mature technique with wide-ranging applications in various industrial processes. In particular, 0.915 ± 0.013 GHz and 2.45 ± 0.05 GHz – the two principal microwave frequencies as assigned by the International Microwave Power Institute (IMPI) – are most often used for industrial, scientific, and medical (ISM) purposes [1]. With its rapid and volumetric internal heating, MW has been used widely to heat, dry, and melt various dielectric (non-conducting) materials, such as paper, concrete, wood, rubber, etc., for the related purposes of tempering frozen meat [2], curing adhesives for lumber [3], quickly heating of food [4–6], bonding composite sheets [7,8], removing contaminated surfaces [9–11], treating hyperthermia [12], and so on.

The use of microwave energy to improve the properties of cement-based materials is a relatively new area of research. However, this is a growing area of interest because microwave heating has many advantages, including high speed for heat generation, high-energy penetration, instantaneous and precise electronic control, and clean process. In addition, conventional heating methods have many limitations. For example, they take a long time to reach the strength required for water curing [13]. In addition, due to the inherent thermal insulation of concrete, they have non-uniform hydration products [13,14]; this causes different temperatures to occur in processed concrete under high-stream and temperature-heating conditions.

Previous research studies have clearly indicated that heating by microwave can further increase the early-age strength of cementitious materials [15–18]. However, some aspects have not been taken into account. Thus, this paper investigates the dielectric properties of cement-based materials during the initial period of hydration at a frequency of 2.45 GHz. The investigation uses a network analyzer with an open-ended probe technique based on the influences of water-to-cementitious ratios, cement types, pozzolan materials, and aggregates. Secondly, this paper examines the characteristics of hardened cement paste at 24-h first hydration when the paste has been subjected to a single-mode rectangular wave guide at a frequency of 2.45 GHz.

2. Experimental

2.1. Materials

Types I and III hydraulic Portland cements were used throughout this test. Their chemical compositions and physical properties are shown in Table 1. The ASTM C 618 [19] classifies the PFA as low calcium (Type F).

☆ Communicated by W.J. Minkowycz.

* Corresponding authors. Research Center for Microwave Utilization in Engineering (R.C.M.E.), Department of Mechanical Engineering, Faculty of Engineering, Thammasat University, (Rangsit Campus), Khlong Luang, Prathum thani, 12121, Thailand.
E-mail address: ratphadu@engr.tu.ac.th (P. Rattanadecho).

0735-1933/$ – see front matter © 2010 Elsevier Ltd. All rights reserved.
doi:10.1016/j.icheatmasstransfer.2010.06.029

Silica fume (hereinafter referred to as SF) was also used as a high-pozzolanic material in accordance with the ASTM C 1240 [20].

Tap water with a pH 7.0 and river sand with a fineness modulus of 2.58 and gradation conforming to the ASTM C 33 [19], were mixed in specific proportions. The chemical admixture used superplasticizer that conforms to the ASTM C 494 [19]; that is, the superplasticizer had a recommended dosage rate of 500 ml per 100 of a kilogram of cementitious materials. Mineral admixtures included pulverized fuel ash (hereinafter referred to as PFA) from an electricity power plant that used lignite coal as a raw material to produce a combustion-yielding steam for driving the generator.

The proportions of cementitious materials mixed in preparation for sample testing are shown in Table 2.

2.2. Sample preparation

Three groups of 117 samples with a cubical shape in size of $55 \times 55 \times 110\ mm^3$ were each tested for dielectric properties, temperature increase, and setting time.

For microwave heating, 24 samples of 0.38 w/c hardened cement paste at the age of 24 h were tested. Each one had dimensions of $55 \times 55 \times 110\ mm^3$. Type I Portland cement and tap water were consistently mixed in accordance with the standard procedures set out in ASTM C 305 [20]. The water-to-Type I Portland cement was kept constant at 0.38 by weight throughout the test. The paste was placed in a mold, which was then wrapped in a plastic sheet to prevent water from evaporating out of the paste. At 24 h after mixing, the samples were de-molded; half were then cured by microwave energy, while the others were cured by water at a temperature of 25.0 ± 2.0 °C.

2.3. Test procedures

In this study, first, the dielectric properties including relative dielectric constant ε' and relative dielectric loss ε'' of cementitious materials during a 24-hour first-hydration period were measured at a frequency of 2.45 ± 0.05 GHz. Second, the characteristics of hardened cement paste as subjected to heating for a short period (without loss of moisture) by microwave energy with a single-mode rectangular wave guide was investigated experimentally and numerically.

To measure the dielectric properties of cementitious materials at a frequency of 2.45 GHz, a network analyzer with an open-ended coaxial probe [21], as shown in Fig. 1, was used. The analyzer consisted of a coaxial cavity; microwave reflectometer; 3.5-mm coaxial cable; 3.5-mm female calibration; and short-, open-, matched-load software. The coaxial cavity characterizes measurement in the range of 1.5–2.6 GHz with precision not more than 2% of the dielectric constant and 5% of the dielectric loss factor. The measured sample should be assumed; i.e., it should be assumed to have infinite size, non-magnetic material, isotropic and homogeneous properties. In addition, the coaxial cavity must be in contact with the sample under test (MUT). The Nicholson-Ross-Weir conversion process [22] was used to calculated dielectric properties. After the cementitious material had been mixed and placed in the mold, it was wrapped in Styrofoam that was 5.0 mm thick in order to protect it from heat loss. Both dielectric properties and semi-adiabatic temperature using a data logger with thermo-couple (Type K) was simultaneously recorded every 180 and 15 min, respectively. However, in order to eliminate the effect of the thermo-couple embedded in microwave radiation, three samples were separately tested for dielectric properties and three for temperature rise. Furthermore, the setting times of pastes, mortars, and cementitious materials were tested by Vicat needle, modified Vicat needle, and penetration resistance in accordance with ASTM C 191 [20], ASTM C 807 [20], and ASTM C 403 [19], respectively.

The microwave system used was a monochromatic microwave at a frequency of 2.45 GHz, as shown in Fig. 2 [23]. Microwave energy was generated by a magnetron and transmitted directly along the propagation direction $(+z)$ of a rectangular wave guide toward a water load situated at the end of the waveguide to ensure that a minimal amount of microwave energy would be reflected back to the sample. A warming water load was circulated through the cooling tower in order to reduce the temperature in the water load system.

A cement paste sample was arranged perpendicular to the propagation direction. A Type K thermo-couple with a 0.1 mm diameter was inserted at the center of the sample for the purpose of monitoring the temperature rise. During a 15-minute period of microwave heating, the output of the microwave magnetron was controlled at 1000 W. The microwave plane wave traveled directly along the wave guide and made contact with the sample surface; the wave was then reflected and transmitted. By using a wattmeter, incident, reflected and transmitted waves were monitored.

The microwave-heated and water-cured samples were each tested for compressive strength at the ages of 3, 7, 14, and 28 days, in accordance with ASTM C 39 [19].

3. Analytical investigation

In order to analyze heat generation by microwave energy inside the hardened cement paste, electromagnetic distribution inside a rectangular wave guide and thermal models were taken onto account. An electromagnetic plane wave in TE_{10} mode was taken into account for calculating the electric-magnetic fields. Since a microwave of the TE_{10} mode propagates uniformly in y-direction, the electromagnetic field can

Table 1
Chemical composition and physical properties of Type I and Type III Portland cements and pulverized fuel ash (PFA) and silica fume (SF).

Chemical composition (% by mass)	SiO_2	Al_2O_3	Fe_2O_3	CaO	MgO	K_2O	Na_2O	SO_3	TiO_2	Free CaO
Type I Portland cement	20.84	5.22	3.20	66.28	1.24	0.22	0.10	2.41	0.25	0.99
Type III Portland cement	19.79	5.33	3.02	65.16	1.37	0.32	0.06	3.65	0.23	0.95
Pulverized fuel ash (PFA)	42.10	21.80	11.22	13.56	2.41	1.38	2.90	1.88	0.44	1.44
Silica fume (SF)	97.50	0.40	0.10	0.20	0.10	0.30	0.10	0.20	0.04	0.08

Physical properties	Type I Portland cement	Type III Portland cement	Pulverized fuel ash (PFA)	Silica fume (SF)
Loss on Ignition (%)	0.96	0.82	2.33	0.59
Moisture Content (%)	0.19	0.14	1.50	0.01
Blaine Surface Area (cm^2/g)	3200	3600	2850	25,600
Fineness (Particle Size, % Retained)				
$-\geq 75$ μm	0.50	0.14	0.56	0.01
−75 μm	5.25	2.15	8.25	0.02
−45 μm	3.60	3.10	4.76	0.01
$-\leq 36$ μm	90.62	94.61	86.43	99.96
Fineness (Retained) on 45 μm (No. 325)	5.75	9.22	4.90	1.09
Water Requirement (%)	100	103	97	108
Bulk Density (kg/l)	1.03	1.12	0.51	0.43
Specific Gravity	3.15	3.16	2.13	2.24

Table 2
Mixing proportions of pastes, mortars and concretes.

Mix symbol	W/C	A/C	Material constitutes (Air content designed = 1.0%)					
			Cement	Pulverized fuel ash	Silica fume	Water	Sand	Crushed Lime stone Rock
			(kg/m^3)	(kg/m^3)	(kg/m^3)	(kg/m^3)	(kg/m^3)	(kg/m^3)
CPI0.38	0.38	0	1417	0	0	538	0	0
CPI0.45	0.45	0	1290	0	0	579	0	0
CPI0.70	0.70	0	973	0	0	679	0	0
CPIII0.38	0.45	0	1419	0	0	539	0	0
CPI0.38SF25	0.38	0	1018	0	337	512	0	0
CPI0.38PFA25	0.38	0	998	335	0	507	0	0
MI0.38	0.38	2.75	561	0	0	212	1546	0
MIII0.38	0.38	2.75	561	0	0	212	1546	0
MI0.38SUPS2.75	0.38	2.75	561	0	0	207	1544	0
MIII0.38SUPS2.75	0.38	2.75	561	0	0	207	1543	0
CI0.38SUP	0.38	4.33	425	0	0	160	805	1030
CI0.45SUP	0.45	4.14	425	0	0	189	771	985
CI0.70SUP	0.70	3.48	425	0	0	296	642	830

Remarks: CP, M and C represent cement paste, mortar and concrete, respectively. I and III represent Types of Portland cement. 0.38, 0.45 and 0.70 represent water-to-cementitious materials (cement/Pulverized fuel ash/Silica fume). SF and PFA represent silica fume and pulverized fuel ash, respectively. SUP represents superplasticizer, and 2.75, 4.33, 4.14 and 3.48 represent aggregate-to-cementitious ratio.

be considered on the *x*–*z* plane of a two-dimensional model (Fig. 3). Thus, such correspondent electromagnetic and temperature fields can be contemplated in a two-dimensional model. Fig. 3 illustrates the physical model for the microwave heating of the cement paste using a rectangular wave guide. The proposed model makes the following assumptions [23]:

(a) Cement paste materials (cement plus water) are themselves composed of non-magnetic materials.
(b) The electrical properties of the rectangular wave guide's walls are perfect conductors that can reflect waves completely.
(c) The absorption of microwave energy by air in the rectangular wave guide is negligible.
(d) The effect of the polyethylene sample container on the electromagnetic and temperature fields can be neglected.

In order to analyze the behavior of electric and magnetic fields in the wave guide, fundamental equations governing the fields, that is, Maxwell's equations, are used. As the above-stated assumptions, the electromagnetic field can be written in terms of the component notations of electric and magnetic field intensities as in Eq. (1) [23]:

$$\frac{\partial \vec{E}_y}{\partial z} = \mu \frac{\partial \vec{H}_x}{\partial t}, \frac{\partial \vec{E}_y}{\partial x} = -\mu \frac{\partial \vec{H}_z}{\partial t}, -\left(\frac{\partial \vec{H}_z}{\partial x} - \frac{\partial \vec{H}_x}{\partial z}\right) = \sigma \vec{E}_y + \varepsilon \frac{\partial \vec{E}_y}{\partial t} \quad (1)$$

where $\vec{E}$ and $\vec{H}$ denote the electric field intensity in (volts per meter (V/m)) and magnetic field intensity (amperes per meter (A/m)), respectively. The subscripts (*x*, *y*, and *z*) represent components of vectors in *x*, *y*, and *z* directions, respectively. Further, the permittivity or dielectric constant, ε (farads per meter, F/m), ε_0 is the permittivity of free space (8.85412×10^{-12} F/m), magnetic permeability, μ and electric conductivity, σ are given as in Eq. (2),

$$\varepsilon = \varepsilon_0 \varepsilon_r, \mu = \mu_0, \sigma = 2\pi f \varepsilon (\tan\delta). \quad (2)$$

The composite materials of cement paste are non-magnetic. Therefore, the materials effect is negligible, as is true for most dielectric materials used in microwave heating. The cement paste's magnetic permeability (μ) can be approximated by μ_0 in the free space $\left(4\pi \times 10^{-7} H/m\right)$.

The boundary conditions associated with the physical model as shown in Fig. 3, are as follows [23]:

(a) Perfectly conducting boundaries. Boundary conditions on the inner wall surface of a rectangular wave guide are given by using Faraday's law and Gauss theorem:

$$\vec{E}_t = 0,\ \vec{H}_n = 0 \quad (3)$$

(b) Continuity boundary condition. Boundary conditions along the interface between different materials, for example between air and dielectric material surfaces, are given by using Ampere's law and Gauss theorem:

$$\vec{E}_t = \vec{E}_t^{'}, \vec{H}_t = \vec{H}_t^{'}, \vec{D}_n = \vec{D}_n^{'}, \vec{B}_n = \vec{B}_n^{'} \quad (4)$$

(c) Absorbing boundary condition. At both ends of the rectangular wave guide, the first-order absorbing conditions are applied:

$$\frac{\partial \vec{E}_y}{\partial t} = \pm \upsilon \frac{\partial \vec{E}_y}{\partial z}. \quad (5)$$

The symbol $\pm$ represents forward or backward waves, and υ is the phase velocity of the microwave (m/s).

(d) Oscillation of the electric and magnetic field intensities by magnetron. The incident wave due to the magnetron is given by the following equations:

$$E_y = E_{yin} \sin\left(\frac{\pi x}{L_x}\right) \sin(2\pi f t), H_x = \frac{E_{yin}}{Z_H} \sin\left(\frac{\pi x}{L_x}\right) \sin(2\pi f t) \quad (6)$$

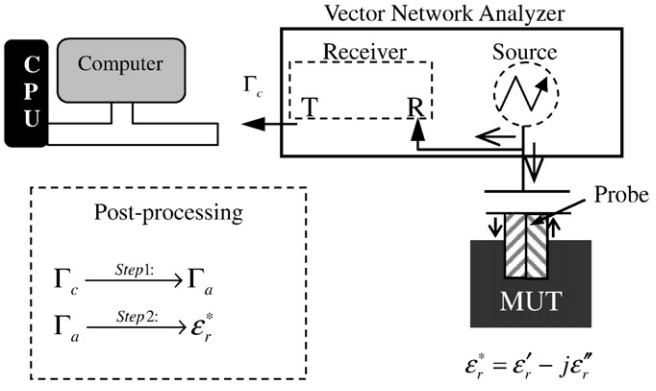

Fig. 1. A network analyzer (open ended probe technique) (R = reflected power, T = transmitted power).

Z_H is the wave impedance defined as:

$$Z_H = \frac{\lambda_g Z_I}{\lambda_0} = \frac{\lambda_g}{\lambda_0}\sqrt{\frac{\mu_0}{\varepsilon_0}}. \tag{7}$$

The finite difference time domain method was applied to predict the electric and magnetic fields; the leapfrog scheme was implemented using Maxwell's equations. The electric field vector components were offset one half cell in the direction of their corresponding components, while the magnetic field vector components were offset one half cell in each direction orthogonal to their corresponding components. The electric and magnetic fields were both evaluated at every other half-time step. For the TE_{10} mode, the electric field and magnetic field components are expressed with the total field FDTD equations thus:

$$E_y^n(i,k) = \frac{1-\frac{\sigma(i,k)\Delta t}{2\varepsilon(i,k)}}{1+\frac{\sigma(i,k)\Delta t}{2\varepsilon(i,k)}}E_y^{n-1}(i,k) + \frac{1}{1+\frac{\sigma(i,k)\Delta t}{2\varepsilon(i,k)}}\frac{\Delta t}{\varepsilon(i,k)} \times\left\{\frac{-\left(H_z^{n-1/2}(i+1/2,k)-H_z^{n-1/2}(i-1/2,k)\right)}{\Delta x} + \frac{\left(H_x^{n-1/2}(i,k+1/2)-H_x^{n-1/2}(i,k-1/2)\right)}{\Delta z}\right\}$$

$$H_x^{n+1/2}(i,k+1/2) = H_x^{n-1/2}(i,k+1/2) + \frac{\Delta t}{\mu(i,k+1/2)}\left\{\frac{E_y^n(i,k+1)-E_y^n(i,k)}{\Delta z}\right\}$$

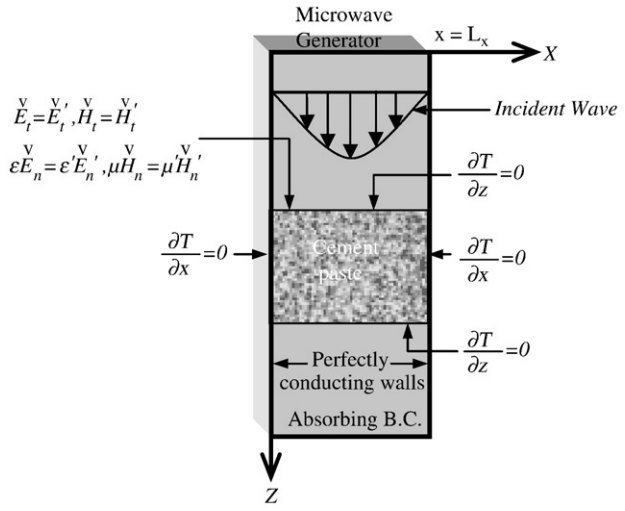

Fig. 3. The electromagnetic field distribution on *x–z* plane and a physical model.

$$H_z^{n+1/2}(i+1/2,k) = H_z^{n-1/2}(i+1/2,k) - \frac{\Delta t}{\mu(i+1/2,k)}\left\{\frac{E_y^n(i+1,k)-E_y^n(i,k)}{\Delta x}\right\}. \tag{8}$$

The temperature rise of the processed cement paste under soaking with microwave can be obtained by solving the heat-conduction transport equation with microwave power included as a local electromagnetic heat-generation term:

$$\frac{\partial T}{\partial t} = a\left(\frac{\partial^2 T}{\partial x^2} + \frac{\partial^2 T}{\partial z^2}\right) + \frac{Q}{\rho \cdot C_p} \tag{9}$$

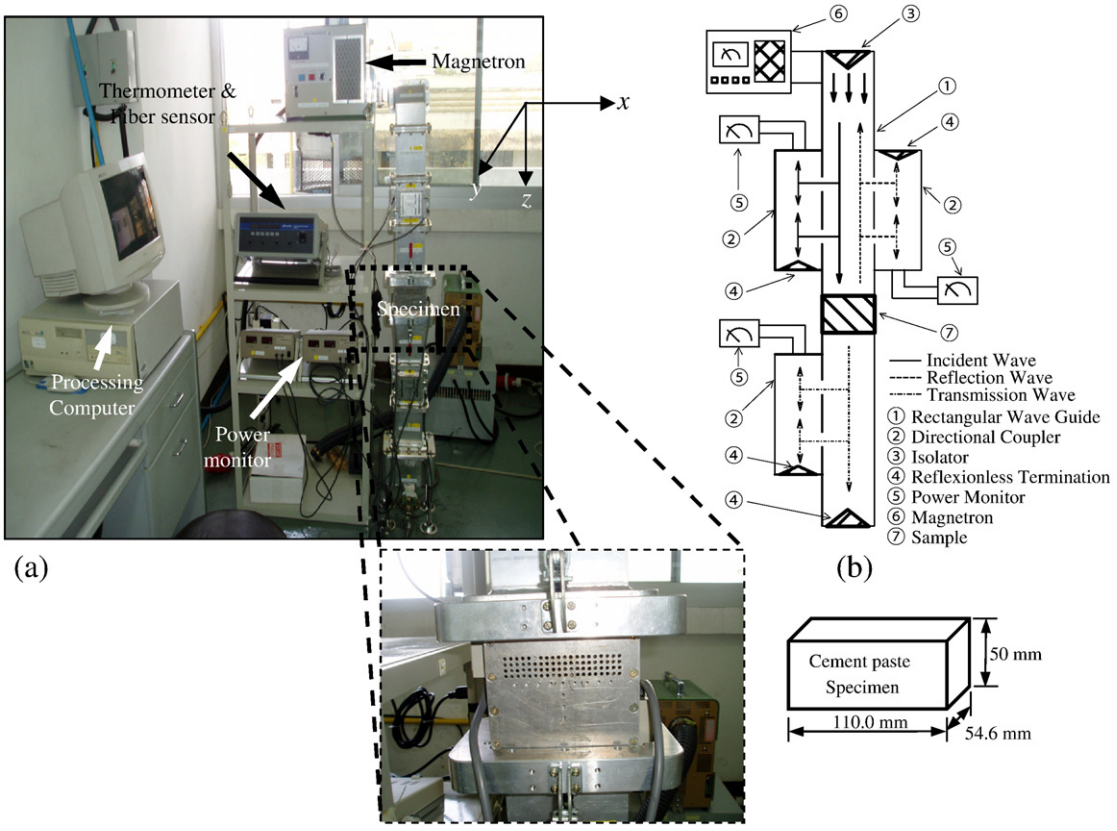

Fig. 2. (a) Experimental set up and (b) schematic showing direction of microwave components (Incident wave, reflected wave, and transmission wave).

where T is the temperature (°C), a is the thermal diffusivity (m^2/s), ρ is the density (kg/m^3), and c_p is the heat capacity at constant pressure ($J/(kg \cdot K)$). The local electromagnetic heat-generation term Q depends on the electric field distribution defined as in Eq. (10):

$$Q = \sigma E^2 = 2\pi f \varepsilon_0 \varepsilon_r' (\tan\delta) E^2 \tag{10}$$

where Q is the microwave energy (W/m^3), σ is the effective conductivity (S/m), f is the frequency (Hz), ε_0 is the permittivity of free space (F/m) (8.85142×10^{-12} F/m), ε_r' is the relative dielectric constant (dimensionless), *tan* δ is the loss tangent coefficient (dimensionless), and $\vec{E}$ is the electric field intensity (V/m).

When microwave energy travels towards the dielectric materials, its wave strength fades away exponentially; this occurs because microwave energy is absorbed into dielectric materials and changes to heat. In general, the penetration depth (D_p) denotes the depth at which microwave power density has decreased to 37% or ($1/e$) of its initial value, as defined in Eq. (11).

$$D_p = \frac{1}{(2\pi f/\upsilon)\sqrt{\left[\varepsilon_r'\left(\sqrt{1 + (\varepsilon_r''/\varepsilon_r')^2} - 1\right)\right]/2}} = \frac{1}{(2\pi f/\upsilon)\sqrt{\left[\varepsilon_r'\left(\sqrt{1 + (\tan\delta)^2} - 1\right)\right]/2}} \tag{11}$$

where D_p is the penetration depth (m), ε_r'' is the relative dielectric loss factor (dimensionless), and υ is the microwave speed in the dielectric material that can be evaluated by $C / \sqrt{\varepsilon_r'}$ (m/s).

The initial condition of the multi-layered materials was defined as $T = T_0$ at $t = 0$, the boundary conditions for solving the heat transport equation can be applied by assuming that all sides of the microwave-assisted heating sample were isolated as shown in Eq. (12) [23].

$$\delta T / \delta n = 0 \tag{12}$$

The heat transport equation (Eq. (9)) was solved by the method of finite volume. The spatial and the temporal terms are approximated using finite difference equations for the electromagnetic field and temperature field. The heat transport equation was discretized and solved on this grid system [23]. The choice of spatial and temporal resolution was motivated by considerations of stability and accuracy. To ensure the stability of the time-stepping algorithm, Δt must be chosen to satisfy the courant stability condition:

The calculation conditions that correspond to Eqs. (13) and (14), were described as follows [23]:

(a) Each wavelength of the microwave in the computational domain with a frequency of 2.45 GHz has more than 10 subdivisions in the numerical calculation. Thus, the computational domain is conservatively set, such that the spatial resolution of each cell is $\Delta x = \Delta z \le \lambda_{mg}/10\sqrt{\varepsilon_r} \approx 1.0$ mm. Thus, the total 110×250 cells in the computational domain were used in the numerical calculation.

(b) Because the propagating velocity of a microwave is very fast as compared with the rate of heat transfer, the different time steps of $dt = 1$ [ps] and 1[s] are used for the computation of the electromagnetic field and temperature field, respectively. The spatial step size is $dx = dz = 1.0$ mm:

$$\Delta t \le \frac{\sqrt{(\Delta x)^2 + (\Delta z)^2}}{\upsilon}. \tag{13}$$

The spatial resolution of each cell is defined as:

$$\Delta x, \Delta z \le \frac{\lambda_g}{10\sqrt{\varepsilon_r}} \tag{14}$$

(c) Number of grid: $N = 110$ (width) $\times 250$ (length).

(d) Relative errors in the iteration procedure of 10^{-8} were chosen.

4. Experimental results and discussion

The dielectric properties of cementitious materials during a 24-hour first-hydration period were measured at a frequency of 2.45 ± 0.05 GHz. First, the dielectric properties of cement paste constituents are described in Section 4.1. In the Section 4.2, the dielectric properties of cementitious materials — that is paste, mortar and concrete with various proportions are presented.

4.1. Dielectric properties of the constituents of cementitious materials

Table 3 shows dielectric properties as a function of the temperature of all cement-based constituents. Generally, dielectric properties consist of dielectric constant ε' and dielectric loss factor ε'' as a function of temperature change. It can be separated into three groups of materials including the following:

(a) The powder material group comprises Portland cement Types I and III, silica fume, and pulverized fuel ash. This group shows a narrow range of dielectric constant and loss tangent throughout the temperature range of 30–80 °C. However the loss factor ε'' of the materials has a wide variation that is greater that its dielectric constant; this is due to having a high variation and it is related to the conductivity of a material's polarization and relaxation behaviors [1].

(b) The water-based materials group consists of water and superplasticizer (polycarboxylic water-based). It has a reasonably wide range of both properties. This is because water is a high lossy material corresponding to with ε' and *tan* δ much higher than that of the other components [1]. This effect shows clearly in chemical admixtures that consist mainly of water and polymer. In fact, the manufacturer specified that the solid content of superplasticizer is 40% by weight. Thus, the dielectric properties of admixtures are strongly influenced by water content.

(c) The aggregate materials group, for example, the fine aggregate (river sand) and the coarse aggregate (crushed limestone rock), has dielectric properties that are narrower than those of the powder and water-based material groups. For the dielectric constant under the same compaction condition, fine aggregate materials show a lower value than powder materials because the former is looser in its consistency.

4.2. Dielectric properties of cementitious materials

Continuity to the aforementioned section, the dielectric properties of cementitious materials are strongly affected by their constituents and mix proportion characteristics. Understanding in their constituents is a basic knowledge to deeply describe when they are mixed together, and hydration and pozzolanic reactions are then took place and also affected backward to the statue the constituents. In this section, the latter factor is discussed in detail including the influences of water-to-cementitious materials, cement types, pozzolan materials and aggregates.

4.2.1. Effect of water-to-cementitious materials

Fig. 4 shows the evolution of relative dielectric properties (ε' and ε'') and the simultaneous temperature rise in cementitious materials. It can be observed that the relative dielectric properties at the initial stage are

Table 3
Dielectric constant (ε') and dielectric loss factor (ε'') of constituents.

Constituents	Dielectric constant (ε'); $\varepsilon'(t) = at^3 + bt^2 + ct + d$			
	$a \pm$ s.d.	$b \pm$ s.d.	$c \pm$ s.d.	$d \pm$ s.d.
Portland cement Type I	−3.671E−07 ± 1.276E−06	3.529E−05 ± 1.869E−04	−2.014E−03 ± 8.294E−03	3.712E+00 ± 4.803E−01
Portland cement Type III	−1.122E−07 ± 1.599E−06	4.021E−05 ± 1.007E−04	−1.476E−03 ± 5.356E−03	6.023E+00 ± 3.911E−01
Pulverized fuel ash	3.333E−07 ± 3.215E−06	−6.667E−05 ± 5.508E−04	4.200E−03 ± 2.859E−02	4.138E+00 ± 3.109E−01
Silica fume	−3.500E−07 ± 7.071E−08	5.500E−05 ± 2.121E−05	−3.350E−03 ± 1.344E−03	2.217E+00 ± 1.790E−01
Superplasticizer (polycarboxylic water-based)	−2.333E−05 ± 8.083E−05	4.767E−03 ± 9.935E−03	−3.260E−01 ± 2.989E−01	2.865E+01 ± 1.933E−01
Fine aggregate (River sand)	−1.000E−08 ± 7.000E−08	−2.333E−06 ± 1.079E−05	2.333E−04 ± 6.429E−04	2.600E+00 ± 1.565E−01
Coarse aggregate (Crushed limestone rock	−8.500E−08 ± 1.626E−07	2.600E−05 ± 4.808E−05	−1.950E−03 ± 3.606E−03	1.224E+00 ± 1.409E−01
Cementitious constituents	Dielectric loss factor (ε''); $\varepsilon''(t) = et^3 + ft^2 + gt + h$			
	$e \pm$ s.d.	$f \pm$ s.d.	$g \pm$ s.d.	$h \pm$ s.d.
Portland cement Type I	3.333E−08 ± 4.989E−08	−7.667E−06 ± 1.115E−05	5.000E−04 ± 7.874E−04	1.565E−01 ± 1.844E−02
Portland cement Type III	7.987E−08 ± 3.043E−08	−3.008E−06 ± 9.453E−06	6.225E−04 ± 2.114E−04	3.922E−01 ± 1.042E−02
Pulverized fuel ash	−1.800E−07	2.650E−05	−1.500E−03	2.763E−01
	3.111E−07	4.738E−05	2.687E−03	7.092E−02
Silica fume	−3.667E−07 ± 2.082E−07	6.333E−05 ± 3.512E−05	−3.733E−03 ± 1.850E−03	2.223E−01 ± 2.045E−02
Superplasticizer (polycarboxylic water-based)	−2.000E−05 ± 1.414E−05	3.400E−03 ± 1.273E−03	−1.664E−01 ± 5.155E−02	9.635E+00 ± 1.025E+00
Fine aggregate (river sand)	7.000E−08 ± 1.224E−08	−2.000E−05 ± 2.633E−06	1.000E−03 ± 1.467E−04	2.645E−01 ± 6.209E−2
Coarse aggregate (crushed limestone rock)	7.000E−09 ± 1.453E−09	−2.000E−06 ± 8.2006E−07	1.000E−04 ± 4.798E−05	5.680E−02 ± 4.334E−03

Remark: *s.d.* = Standard Deviation.

relatively high in comparison with the later stage; it also increases with the increasing water content (higher w/c) of the cementitious material. This is due to the fact that immediately after contact has been made between water and cement, they start to react and then Ca^{2+}, OH^-, and SO_4^{2-} ions dissolve into the system. In addition, during the dormant period, the dielectric properties changes very little because the chemical compositions of the aqueous remain nearly constant [24]. Similarly, relative dielectric properties also appear to be affected by the temperature rise. The lower temperature (higher w/c) leads to the higher these properties. This is due to a reduction in water-to-cement-ratio accelerates hydration and results in higher temperature. Especially, in the accelerated period of the pastes at which has the highest increasing rate of temperature rises corresponds to the highest decreasing rate of relative dielectric properties.

4.2.2. Effect of cement types

Fig. 5 shows the changes of dielectric properties throughout the early stage of the 24 h hydration reaction period. Dielectric properties remain at a high level throughout the dormant period; however, it decreases at the end of this period, approaching a constant value when the internal structure has stabilized. The dielectric properties of Type III pastes is higher than that of Type I paste because Portland cement Type III has finer tri-calcium aluminate (C_3A) grains [25] than Type I. This causes Portland cement Type III to dissolve at a high rate and to maintain an ion-rich system. In addition, the decreasing rate at which the dielectric properties of Type III paste is higher than that for Type I. In the acceleratory period, the Type III paste reacts faster than the Type I paste. This coincides with the evolution of temperature rise and shorter dormant period. It is also seen that the changes in the slope of decreasing

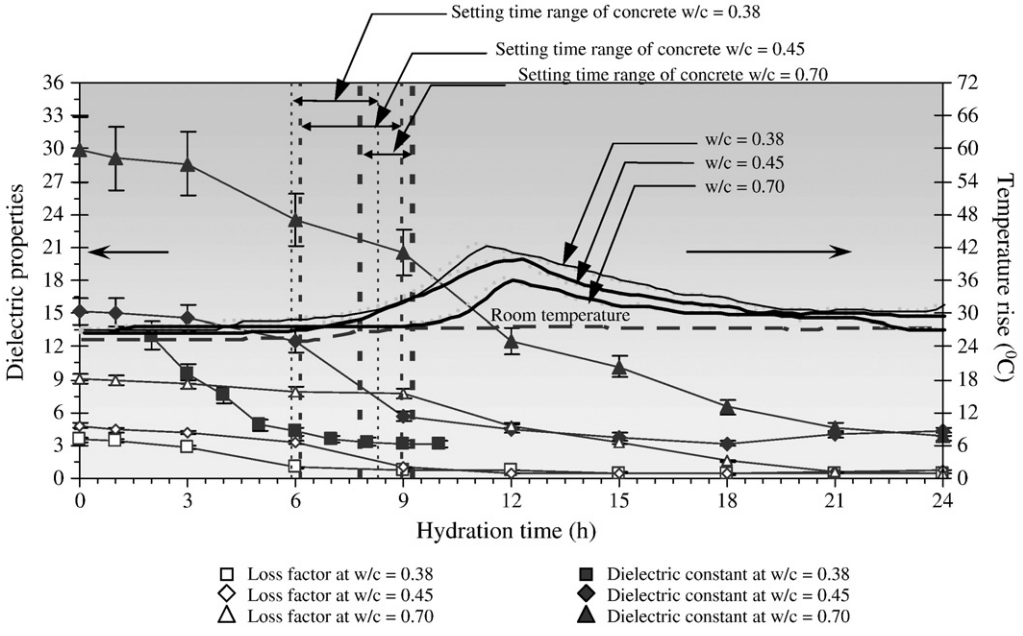

Fig. 4. Dielectric properties of concretes with different w/c ratios.

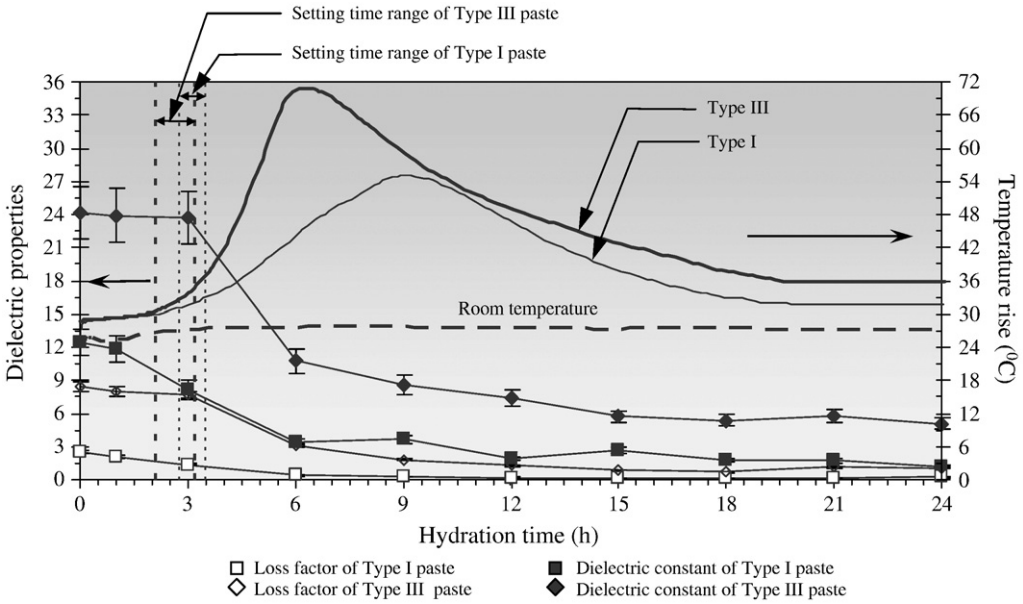

Fig. 5. Dielectric properties of pastes with different cement types.

rate of dielectric properties relate to the rate of temperature rise, the Portland cement Type III>Portland cement Type I. For setting time, the dielectric constant is maintained until the final setting time because of the high dissolution rate; however, the dielectric constant drops dramatically with the high hydration rate. At the later stage after formation of the C–S–H structure, the dielectric properties tend to remain constant because of the strong constraints imposed by its structure.

4.2.3. Effect of pozzolan materials

Effects of silica fume (SF) and pulverized fuel ash (PFA) on the relative dielectric properties, temperature rise, and setting time of the pastes are shown in Fig. 6. The relative dielectric constant of the paste containing PFA through the first 24 h hydration time is higher than that of the plain paste, whereas the paste containing SF is lower. Both reactions involving SF and PFA occur as secondary reactions. This means, however, that the PFA can produce excessive water in the paste while increasing Si^{3+} and Ca^{2+} ions in the system. This results in an increasing relative dielectric constant of the paste. Unlike the SF paste, the compositions with PFA can dissolve at a high rate; its fineness induces the bounding of its water molecules and ion-richness at the surface. As a result, the dielectric constant is lower than that of the plain cement paste. For loss factor evolution, the conventional paste and the SF paste show little difference in their comparative loss factors; however between, the difference in the loss factors of the conventional and SF paste when compared with the PFA paste is large. This indicates that the remaining water content, both during introduction and acceleratory periods in the paste, has a strong effect on dielectric loss. On the other hand, the PFA particles can retain free water in the paste system, which may cause the loss factor of the PFA paste to become very high.

When consider the relationship between the temperature rise of the pastes and the relative dielectric properties, it can be seen that the change in slope are also consistent with the changes in the characteristic feature observed in the temperature rise. However,

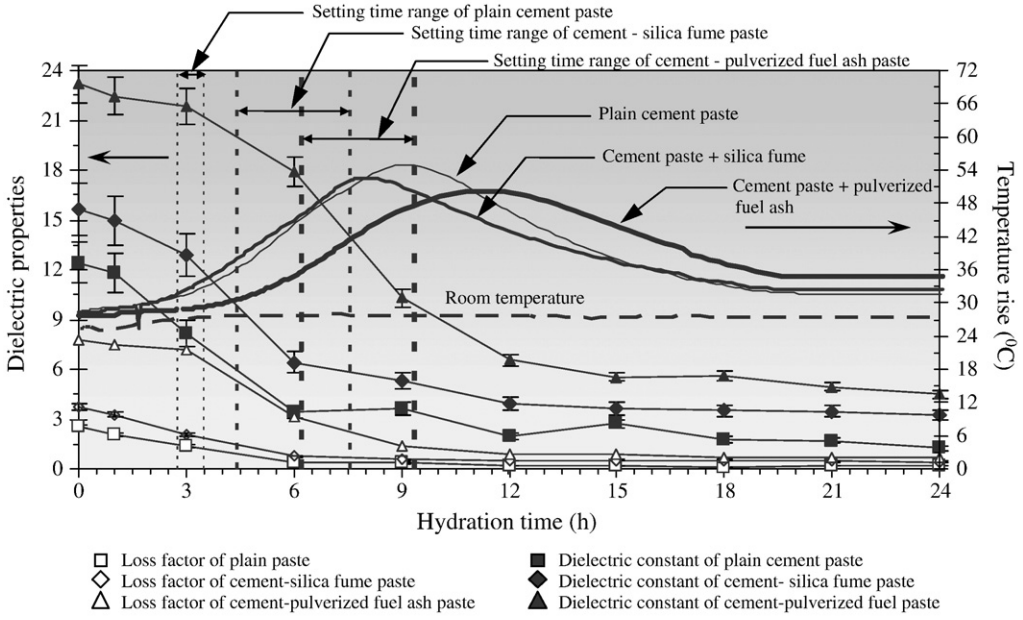

Fig. 6. Dielectric properties of pastes with different pozzolan materials.

they are based on that the higher rate of increase in temperature, the higher rate of decrease in the relative dielectric properties.

4.2.4. Effect of aggregates

Fig. 7 shows that the relative dielectric properties curves for the mortar and concrete are also similar to the curve of the plain paste but lower than that of the paste. The decrease of cement content and the absorption of water molecules by aggregate surfaces induce a lower concentration of ions in the system [25]. However, eventually, these parameters approach to constant. A comparison in the setting time range shows that the paste's relative dielectric properties decrease rate slope is somewhat higher than those of mortars and cementitious materials. This is due to the ion constraints of the hydrated products; specifically that the hydrated products have high ion content in comparison with the aggregate-mixed products.

As discussed on the effect of temperature on the relative dielectric properties in the above section, the concrete sample is lower temperature rise than the mortar and plain cement paste, respectively. The changes of the relative dielectric properties of concrete is low sensitivity with temperature change when comparison with the paste and mortar.

4.3. Temperature rise with the hardened cement paste sample during heating by microwave energy

Fig. 8 shows the temperature history taking place at the center of the hardened cement paste sample that has the age of 24 h after mixing during microwave heating at 1000 W for 15 min. It can be seen that temperature continuously increased when the time for microwave heating increased; the temperature increased at a high rate during the early heating period (the first 1 min) and decreased rapidly during the later heating period (after 1 min). It is mainly caused by the effect of the amount of water content at the surface of sample. This means that at early time, high water content which has a high inherent of dielectric strength by itself, can cause heat generation to take place within the sample with high level. Furthermore, the temperature rise within the sample at the early stage increases dramatically along the propagation direction because of the skin depth heating effect.

4.4. Compressive strength

Fig. 9 shows the strength development of cement paste after microwave heating as compared to water curing. It can be seen that cement paste cured by microwave has higher strength than the cement paste cured by water. The compressive strengths of both microwave-heated and water-cured cement paste increase quickly from day 1 until day 7. From the figure, the early-age strength of microwave-heated cement paste is clearly superior than the early-age strength of the water cured cement paste. The results indicate that microwave application can significantly increase the degree of hydration during the first few days, after which the microwave-heated samples and the control sample attain a similar degree of hydration. After 7 days, the strength appears to become constant; while in the long term the strengths of each of the microwave-heated samples is slightly lower than for the water-cured samples. This is because microwave-heated cement pastes at short time exhibit fewer microcracks; this corresponds to a better micro structure arrangement, and it improves compressive strength [25]. However, after 14 days crossover behavior occurs in regard to the relative strength of the water-cured and microwave-heated cement paste samples. This takes place due to high early hydration of cement under conditions of overheating. In turn, the overheating may produce a large amount of very fine calcium silicate hydrate (C–S–H) gel, which coats the unhydrates and so hinders diffusion and crystallization of the products of the hydration reactions. These reactions consequently affect the development of long term-strength [26].

The maturity index can be approved based on the Arrhenius equation used to describe the effect of temperature on the rate of a chemical reaction. Thus, the equivalent age (t_e) of cement-based materials is set as follows [26]:

$$t_e = \sum_{t=0}^{t=t} e^{\frac{-E}{R}\left(\frac{1}{T(K)}-\frac{1}{T_r(K)}\right)}\Delta t \tag{15}$$

where t_e is the equivalent age, E is the apparent activation energy (J/mol) [27,28], R is the universal gas constant (8.314 J/mol. °K), T is the average absolute temperature of cementitious material during time interval Δt (°K), and T_0 is the absolute reference temperature (23 °C).

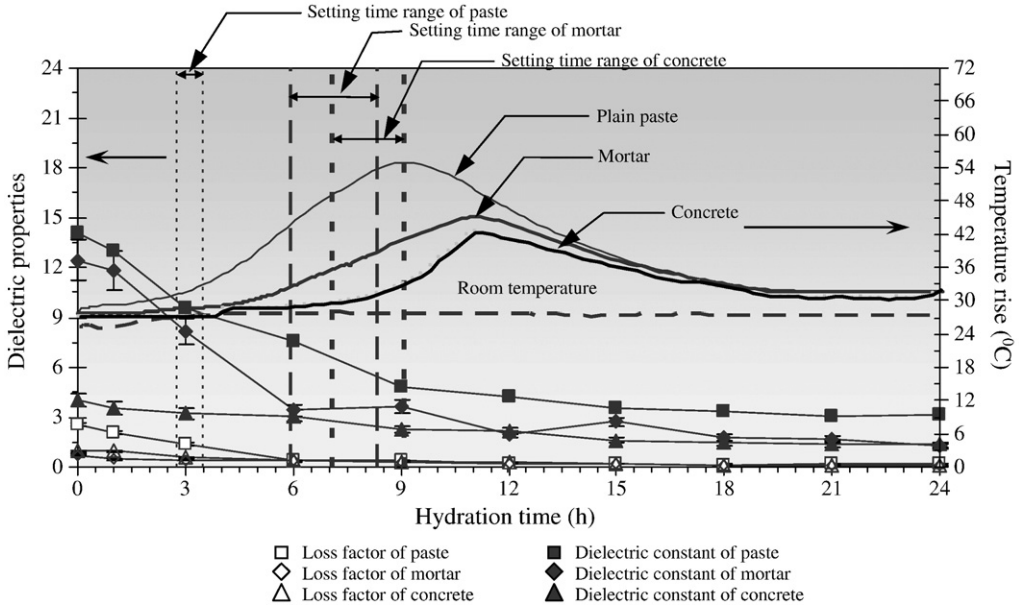

Fig. 7. Dielectric properties of paste, mortar and concrete.

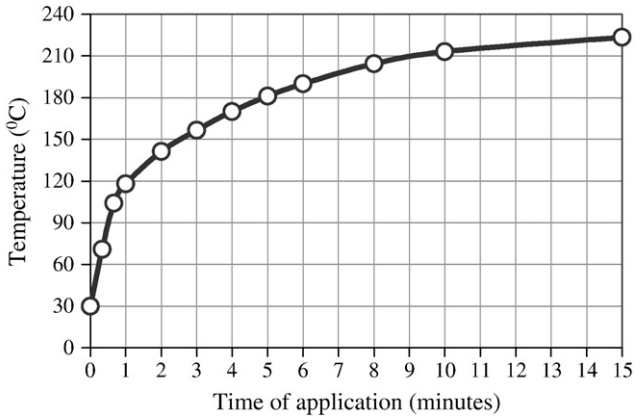

Fig. 8. Temperature rise at the center of the hardened cement paste sample during heating by microwave energy at 1000 W for 15 min.

One simple strength–maturity relationship used the logarithm equation for strength gain under isothermal heating up to an equivalent age at 23 °C for 28 days:

$$S = a + b \cdot \log(M) = a + 2.302 \cdot b \cdot \ln(M) \tag{16}$$

where S is the strength at age t, a is the strength for maturity index ($M=1$), b is the slope of the line, and M is the maturity index.

According to the Eqs. (15) and (16) and the ASTM 1074 [19], the relationship of the strength–maturity index can be expressed as in Eq. (17). Furthermore, Table 4 reports the value of the referred parameters in order to calculate the strength–maturity relationship:

$$t_e = \sum_{t=0}^{t=t} e^{\frac{-E(J/mol)}{8.314(J/mol.K)}\left(\frac{1}{(T(^0C)+273.15)(K)} - \frac{1}{T_r(^0C)+273.15(K)}\right)} \Delta t. \tag{17}$$

A relationship based on an average of three compressive strengths at each test time against the maturity index is shown in Fig. 10. It can be illustrated that a natural logarithm function with coefficients $a=284.4$ and $b=88.2$ constituted a best-fit relationship.

5. Comparison of predictions and experimental results of temperature rise during microwave heating

In the beginning, to understand the detailed structures of electric field developed inside a rectangular waveguide, the numerical simulation of the rectangular waveguide is filled with the heated sample with heating times of 15 min.

Fig. 11(a) shows are the numerical simulation of electric field in TE_{10} mode along the center axis ($x=54.61$ mm) of rectangular waveguide after 10,000 time steps at microwave power 1000 W for 1 min. In the figures, the vertical axis represents the intensity of the electric field E_y, which is normalized to the amplitude of the input electromagnetic wave, E_{yin}. It is shown that the distribution of the electric field when a hardened cement paste is inserted in the rectangular waveguide. Within the sample, the electric field attenuates owing to energy absorption, and the absorbed energy is then converted to the thermal energy, which increases the sample temperature. In the figure, the electric field with a small amplitude is formed within the sample waveguide. Furthermore, focusing attention of field pattern outside the sample (left hand side), a stronger standing wave with a larger amplitude is formed by interference between the forward wave and waves reflected from the surface of sample due to the different of dielectric properties of material (air and sample) at this surface.

Due to high lossy material in the paste at the age of 24 h after the cement particles and water are mixed together, microwaves' penetrating irradiation occurs at a smaller depth than the depth of sample. Consequently, a larger part of the microwaves is absorbed by the sample. It is observed from the figure that the resonance of standing wave configuration inside the small sample is weak.

Fig. 11(b) exhibits temperature in cement paste between heating by microwave energy. The temperature distributions correspond to the electric field distribution in the processed sample. This is because attenuation of the electric field when travels through the sample owing to energy absorption and thereafter the absorbed energy are converted to heat resulted in increase the temperature of the heated cement paste. For example, in addition the temperature distributions are shown for time of application of microwave for 15 min brings about the maximum temperature approaches to around 220 °C. It is observed that the temperature distributions within the paste display a weak wavy behavior due to the penetration depth of microwave drops dramatically and the wavelength is short. Since the reflected wave from the lower surface of the paste is almost negligible, a weak resonance is formed within the paste.

Regarding to tendency of temperature rise within the cement paste, the temperature rise is increased continuously when the heating time of microwave energy increased. The feature trend of temperature increment consists of high rate at the early-age and

Table 4
The values use to calculate the relationship.

Initial conditions	Values
w/c (by weight)	0.38
Temperature	30 °C (303.15 °K)
absolute reference temperature	296.15 °K [25]
Apparent activation energy, E (KJ/mol)	0.685 × (T°C) + 18.117 [27,28]

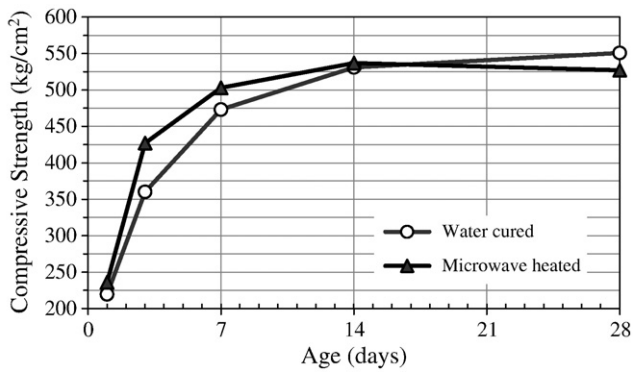

Fig. 9. Comparison of compressive strength development for different heating/curing methods.

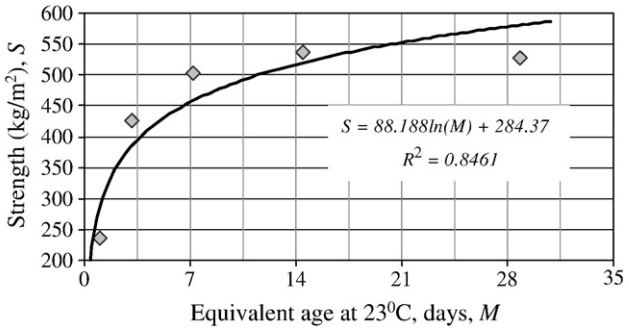

Fig. 10. A strength-maturity relationship of the 0.38-w/c cement paste.

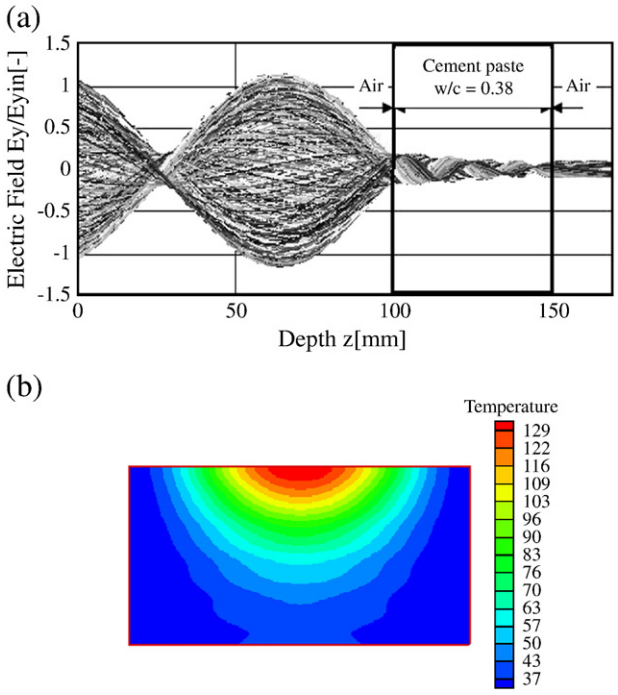

Fig. 11. (a) Distribution of electric field for the hardened cement paste sample inserted in the rectangular waveguide (t = 60 min, x = 54.61 mm, Power = 1000 W) and (b) Temperature distribution (°C).

continuous decrease. It is caused by the effect of penetration depth of absorbed microwave energy and the amount of water content at the surface of the heated sample. This means that before setting of cement paste, the cement particles settled as gravitational force lead to high porosity or capillary pores with soaked surface near contacting surface to microwave energy.

6. Conclusions

The dielectric properties of cement-based materials are affected by initial water-to-cement ratio, cement types, pozzolan, and aggregate types. However, though the volumetric fraction of water and superplasticizer in a given mixture are small, they strongly affect the dielectric properties of the cement. This is because of the high dielectric properties of water and superplasticizer. The change in the dielectric properties is relatively high and remains constant during the dormant period; after that it decreases rapidly when the hydration reaction resumes, and it continues to decrease during the acceleratory period.

Under heating by microwave energy using a rectangular wave guide, at the end of the first 14 days (early age) the compressive strength of the hardened cement paste at water-to-Portland cement by mass ratio of 0.38 had increased and then slightly decreased from 14 to 28 days.

Based on the maturity concept, a relationship between the compressive strength of the hardened cement paste and the maturity index is $Compressive\ Strength = 88.2 \times ln(Maturity\ Index) + 284.4$.

Temperature continuously increased when the time for microwave heating increased. The temperature increased at a high rate during the early heating period (the first 1 min) and then decreased rapidly during the later heating period (after 1 min).

The temperature rise as actually recorded at the center of the sample during microwave heating in our experiment consistently agreed with figures calculated by a mathematical model.

Acknowledgment

The authors gratefully acknowledge the Thailand Research Fund (TRF) for supporting this research project under the Royal Golden Jubilee Program (RGJ) contract No. PHD/0030/2549.

References

[1] A.C. Metaxas, Microwave heating, The Journal of Microwave Power and Electromagnetic Energy (1991) 237–247.
[2] F. Peyre, A. Datta, C. Seyler, Influence of the dielectric property on microwave oven heating patterns: application to food materials, The Journal of Microwave Power and Electromagnetic Energy 32 (1997) 3–15.
[3] F.C. Beall, Industrial applications and opportunities for nondestructive evaluation of structural wood members, Maderas: Ciencia y Tecnologia 9 (2007) 127–134.
[4] H. Chen, Simulation model for moving food packages in microwave heating processes using conformal FDTD method, Journal of Food Engineering 88 (2008) 294–305.
[5] V. Orsat, Microwave-assisted drying of biomaterials, Food and Bioproducts Processing 85 (3C) (2007) 255–263.
[6] J. Zhu, A.V. Kuznetsov, K.P. Sandeep, Numerical modeling of a moving particle in a continuous flow subjected to microwave heating, Numerical Heat Transfer, Part A: Application 52 (5) (2007) 417–439.
[7] N. Sgriccia, M.C. Hawley, Thermal, morphological, and electrical characterization of microwave processed natural fiber composites, Composites Science and Technology 67 (9) (1991) 1986–1991.
[8] T. Basak, S. Durairaj, Numerical simulation on efficient microwave processing of thermoplastics with ceramic composites, Numerical Heat Transfer, Part A: Application 57 (8) (2010) 554–579.
[9] W. Li, M.A. Ebadian, T.L. White, R.G. Grubb, D. Foster, Heat and mass transfer in a contaminated porous concrete slab with variable dielectric properties, International Journal of Heat and Mass Transfer 37 (6) (1994) 1013–1027.
[10] L.E. Lagos, W. Li, M.A. Ebadian, T.L. White, R.G. Grubb, D. Foster, Heat transfer within a concrete slab with a finite microwave heating source, International Journal of Heat and Mass Transfer 38 (1995) 880–897.
[11] Z.P. Bažant, G. Zi, Decontamination of radionuclides from concrete by microwave heating. I: theory, Journal of Engineering Mechanics (2003) 777–784.
[12] K. Arunachalam, Characterization of a digital microwave radiometry system for noninvasive thermometry using a temperature-controlled homogeneous test load, Physics in Medicine and Biology (2008) 3883–3901.
[13] K.Y.C. Leung, T. Pheeraphan, Microwave curing of Portland cement concrete: experimental results and feasibility for practical applications, Construction and Building Materials 9 (1995) 67–73.
[14] R.G. Hutchison, J.T. Chang, H.M. Jennings, M.E. Brodwin, Thermal acceleration of Portland cement mortars with microwave energy, Cement and Concrete Research 21 (1991) 795–799.
[15] M. Moukwa, M. Brodwin, S. Christo, J. Chang, S.P. Shah, The influence of the hydration process upon microwave properties of cements, Cement and Concrete Research 21 (1991) 863–872.
[16] P. Rattanadecho, N. Suwannapum, B. Chatveera, D. Atong, N. Makul, Development of compressive strength of cement paste under accelerated curing by using a continuous microwave thermal processor, Materials Science and Engineering A 472 (2008) 299–307.
[17] T. Pheeraphan, Accelerated curing of concrete with microwave energy, Doctor of Philosophy Dissertation, MIT (1997).
[18] L. Dongxu, W. Xuequan, A study on the application of vacuum microwave composite dewatering technique in concrete engineering, Cement and Concrete Research (1994) 159–164.
[19] American Society for Testing and Materials, Annual Book of ASTM Standard Vol. 4.02, 2009 Philadelphia, PA, USA.
[20] American Society for Testing and Materials, Annual Book of ASTM Standard Vol. 4.01, 2009 Philadelphia, PA, USA.
[21] HP, Dielectric Probe Kit 85070A, Research and Development Unit, Test and Measurements Laboratories, Hewlett Packard Corporation, Palo Alto, CA, 1992.
[22] M.S. Venkatesh, G.S.V. Raghevan, An overview of dielectric properties measuring techniques, Canadian Biosystems Engineering 47 (2005) 15–29.
[23] P. Ratanadecho, K. Aoki, M. Akahori, A numerical and experimental investigation of the modeling of microwave heating for liquid layers using a rectangular wave guide (effects of natural convection and dielectric properties), Applied Mathematical Modelling 26 (3) (2002) 449–472.
[24] P.C. Hewlett, Lea's Chemistry of Cement and Cementitious Material, 4th EditionJohn Wiley & Sons Inc., New York, 1998.
[25] H.F.W. Taylor, Cement Chemistry, 2nd EditionThomas Telford Publishing, Great Britain, 1997.
[26] N. Cario, The maturity method: theory and application, Cement, Concrete & Aggregates (1993) 61–73.
[27] H.K. Benameur, E. Wirquin, B. Duthoit, Determination of apparent activation energy of concrete by isothermal calorimetry, Cement and Concrete Research (2000) 301–305.
[28] L.D. Aloia, G. Chanvillard, Determining the apparent activation energy of concrete E_a — numerical simulations of the heat of hydration of cement, Cement and Concrete Research (2002) 1277–1289.